BIOCHEMISTRY
including biophysical chemistry & molecular biology

Article

pubs.acs.org/biochemistry

Allosteric Inactivation of a Trypsin-Like Serine Protease by An Antibody Binding to the 37- and 70-Loops

Tobias Kromann-Hansen,*[,†,‡] Ida K. Lund,[§,∥] Zhuo Liu,[†,‡] Peter A. Andreasen,[†,‡] Gunilla Høyer-Hansen,[§,∥] and Hans Peter Sørensen[†,‡]

[†]Danish-Chinese Centre for Proteases and Cancer and [‡]Department of Molecular Biology and Genetics, Aarhus University, DK-8000 Aarhus C, Denmark

[§]The Finsen Laboratory, Copenhagen University Hospital, DK-2200 Copenhagen N, Denmark

[∥]Biotech Research and Innovation Centre (BRIC), University of Copenhagen, DK-2200 Copenhagen N, Denmark

Supporting Information

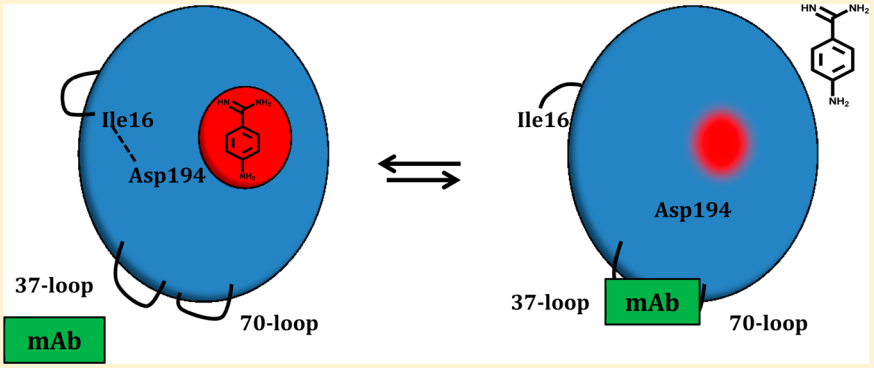

ABSTRACT: Serine protease catalytic activity is in many cases regulated by conformational changes initiated by binding of physiological modulators to exosites located distantly from the active site. Inhibitory monoclonal antibodies binding to such exosites are potential therapeutics and offer opportunities for elucidating fundamental allosteric mechanisms. The monoclonal antibody mU1 has previously been shown to be able to inhibit the function of murine urokinase-type plasminogen activator in vivo. We have now mapped the epitope of mU1 to the catalytic domain's 37- and 70-loops, situated about 20 Å from the S1 specificity pocket of the active site. Our data suggest that binding of mU1 destabilizes the catalytic domain and results in conformational transition into a state, in which the N-terminal amino group of Ile16 is less efficiently stabilizing the oxyanion hole and in which the active site has a reduced affinity for substrates and inhibitors. Furthermore, we found evidence for functional interactions between residues in uPA's C-terminal catalytic domain and its N-terminal A-chain, as deletion of the A-chain facilitates the mU1-induced conformational distortion. The inactive, distorted state is by several criteria similar to the E* conformation described for other serine proteases. Hence, agents targeting serine protease conformation through binding to exosites in the 37- and 70-loops represent a new class of potential therapeutics.

The serine protease urokinase-type plasminogen activator (uPA) can, while bound to urokinase-type plasminogen activator receptor (uPAR) at cell surfaces, catalyze the conversion of the zymogen plasminogen to the active serine protease plasmin. Plasmin catalyzes the degradation of extracellular matrix proteins and up-regulation of uPA is implicated in several physiological and pathophysiological conditions related to tissue remodeling, including wound healing, fibrinolysis, inflammation, embryogenesis, and angiogenesis.[1,2] The uPA system is pleiotropic in the neoplastic processes affecting cancer cell proliferation, tumor angiogenesis, adhesion, invasion, and migration.[1,2] uPA is a potential therapeutic target in cancer, arthritis, and other diseases.[3,4]

uPA consists of an N-terminal A-chain and a C-terminal B-chain. The A-chain of uPA is composed of an N-terminal uPAR-binding growth factor-like domain, a kringle domain, an intradomain linker, and residues 1−15[a] of the catalytic domain. The B-chain encompasses residues 16−250 of the catalytic domain. The A- and B-chains are linked by a disulfide bond between Cys1 and Cys122 (Figure 1). Like other serine proteases, uPA is secreted from cells as a single-chain zymogen, also known as pro-uPA. Cleavage of single-chain uPA between Lys15 and Ile16 can be catalyzed by plasmin and a few other serine proteases.[5,6] In general, cleavage of zymogens between amino acid residues 15 and 16 allows for insertion of the liberated N-terminal Ile16 into the activation pocket, a hydrophobic cleft, in which its amino group forms a stabilizing salt-bridge to Asp194 next to the catalytic Ser195. Conformational rearrangements

Received: April 19, 2013
Revised: July 24, 2013
Published: September 9, 2013

   dx.doi.org/10.1021/bi400491k | *Biochemistry* 2013, 52, 7114−7126

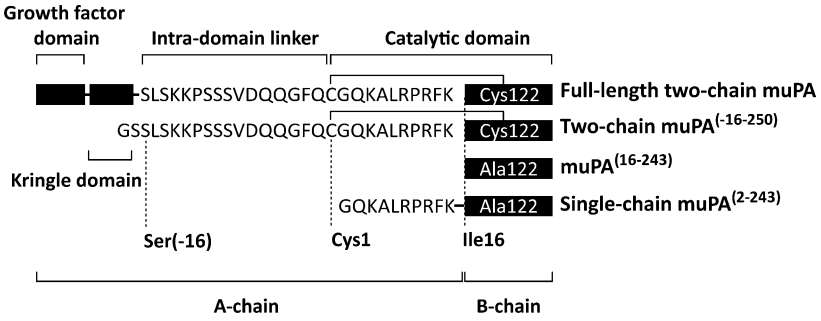

Figure 1. Murine uPA (muPA) and truncation variants. Schematic illustration showing the domain organization of full-length two-chain muPA, the variants two-chain muPA$^{(-16-250)}$, muPA$^{(16-243)}$, and single-chain muPA$^{(2-243)}$, and the sequence in the region between the kringle domain and Ile16. With reference to chymotrypsin, we define the catalytic domain as beginning with Cys1. All variants will initially be secreted from producer cells in the one-chain zymogen form but can be converted to their two-chain counterparts by plasmin-catalyzed hydrolysis of the Lys15−Ile16 bond. In two-chain muPA$^{(-16-250)}$, two additional N-terminal residues, GS, were inserted in front of Ser(-16) to ensure proper signal peptide cleavage. We define the A-chain and the B-chain as the two chains appearing in sodium dodecyl sulfate polyacrylamide gel electrophoresis (SDS−PAGE) of the two-chain forms under reducing conditions.

induced by single-chain zymogen cleavage organize both the S1 specificity pocket and the oxyanion hole of the active site by a mechanism common to all serine proteases.[7−10] Still, in the cleaved as well as uncleaved states, active and inactive forms are in equilibrium. The equilibrium is strongly shifted toward the inactive zymogen in the single-chain form and strongly shifted toward the active protease in the two-chain form. For uPA, the enzyme efficiency ($k_{cat.}/K_M$) for hydrolysis of plasminogen by the single-chain form is at least 250 times lower than that of the two-chain form.[6] The relative enzymatic efficiencies of single- and two-chain forms vary among different serine proteases. While a number of three-dimensional structures of the catalytic domain of human uPA have been solved by X-ray crystallography,[11,12] structures of human and murine single-chain uPA remain to be determined.

Sufficient specificity of small molecule protease inhibitors is difficult to achieve because of the highly conserved active site topologies among related proteases, as clearly illustrated by the difficulties in obtaining potent and selective uPA inhibitors[13] and the severe side-effects and inefficiency of matrix metalloprotease active site inhibitors in clinical trials.[14] These complications have caused increased interest in reagents such as monoclonal antibodies, binding to the less conserved exosites and allosteric sites. Because of their potency and specificity, antibodies are widely used as therapeutic agents, and a total number of more than 35, directed against a variety of targets, have been approved as drugs by the US Food and Drug Administration.[15,16] Antibodies are able to specifically inhibit serine proteases by simple steric hindrance,[17] and even greater efficiency may be achieved by antibodies that conformationally regulate the active site by allosteric mechanisms.[18] Detailed studies of allosteric antibodies against the serine proteases hepatocyte growth factor activator (HGFA), hepsin, and human uPA have elucidated distinct inhibition mechanisms with binding sites as far as 15−20 Å away from the active site.[19−21]

A murine monoclonal antibody, mU1, binding to murine uPA (muPA), can inhibit plasminogen activation in vitro, rescue mice treated with muPA-activatable anthrax pro-toxin, and impair muPA-mediated fibrinolysis as well as delay wound healing in vivo.[22,23] Here, we present the molecular mechanism responsible for mU1-mediated inhibition of muPA. Our analysis revealed that mU1 distorts the active site of muPA, leading to a reduced affinity for substrates and inhibitors, although it binds 20 Å away. The distortion is associated with increased solvent exposure of the amino group of the N-terminal Ile16 of the B-chain. Surprisingly, interactions between the B-chain and Phe(−2) and Lys4 of the A-chain counteract transition into the inactive conformation. The inactive and apparently distorted conformation resembles the inactive E* conformation described for other serine proteases. We have hereby discovered previously unknown communication routes within the catalytic domain of serine proteases that are of general interest, when designing and developing specific and potent serine protease inhibitors.

EXPERIMENTAL SECTION

Monoclonal Antibodies. The generation and characterization of mU1 and mAb-112 were described previously.[22,24]

muPA Production in HEK293 6E Suspension Cells. cDNAs encoding muPA (NP_032899.1, 413 residues without the signal peptide), domain deletion mutants, and site-directed mutants were cloned into the pTT5 or pCDNA3.1 vectors. All variants contained a glycine and six histidines at the C-terminus. The muPA$^{(16-243)}$ and single-chain muPA$^{(2-243)}$ variants contained a C122A mutation, whereas the two-chain muPA$^{(-16-250)}$ variant lacks the amino terminal fragment of muPA (Figure 1). The vectors were transfected into HEK293 6E suspension cells, which were cultured in a humidified CO_2 incubator at 37 °C. The medium used was Freestyle F17 (Gibco) supplemented with 4 mM L-glutamine, 0.1% Pluronic F68 (Gibco), 1% penicillin/streptomycin, 25 μg/mL G418. Linear polyethyleneimine (PEI) (2.2 mg) in cDNA (1.1 mg) in phosphate-buffered saline (PBS; 10 mM sodium phosphate, pH 7.4, 140 mM NaCl) (110 mL) were preincubated for 15 min and added to 1 L of culture with a density of 1 × 10^6 cells/mL. Tryptone N1 (0.5%) was added to the culture 24 h post-transfection. The culture was continued for 6 days before harvesting the conditioned media.

muPA Purification and Characterization. Full-length two-chain muPA wt and variants hereof (i.e., single-chain muPA$^{(2-243)}$, muPA$^{(16-243)}$, two-chain muPA$^{(-16-250)}$, and two-chain muPA$^{(-16-250)}$F(−2)A-K4G)) were purified from conditioned media of transiently transfected HEK293 6E cells. The following alanine substitution muPA mutants were prepared similarly: G37cA, P37eA, P38A, K72A, S74A, Y76A, N77A, and P78A. The proteins, as mentioned above with a glycine and six histidines at the C-terminus, were captured on a nickel−Sepharose column directly from the conditioned media, supplemented with 25 mM imidazole and 50 mM NaCl. The column was washed with 20 mM sodium phosphate, pH 7.4,

dx.doi.org/10.1021/bi400491k | Biochemistry 2013, 52, 7114−7126

0.3 M NaCl, and 25 mM imidazole. The bound protein was eluted from the column with 50 mM bicine, pH 8.0, 0.3 M NaCl, and 0.4 M imidazole. To convert the purified single-chain muPA into its two-chain counterpart, it was incubated at a concentration of 2 μM with 5 nM plasmin for 20 h at 22 °C. Benzamidine−Sepharose chromatography was used to isolate the active fraction, by capturing the proteins on a benzamidine-Sepharose column, which was then washed with 20 mM sodium phosphate, pH 7.4, 0.3 M NaCl, and eluting bound protein with 20 mM sodium citrate, pH 3.0. Protein concentrations were determined using measurements of the absorbance at 280 nm and the theoretical extinction coefficient calculated using the Protparam server located at http://web.expasy.org/protparam/. All preparations were more than 90% pure, as determined by SDS−PAGE (data not shown). The active enzyme concentration, $[E]_{TOTAL}$, was calculated from the absorbance at 280 nM, assuming that the benzamidine−Sepharose-purified product was 100% active. Glutamyl-glycyl-arginyl-chloromethyl ketone (EGR-cmk), at a concentration of 1 mM, was covalently coupled to muPA (at a concentration of 1 μM) by incubation for 3 h at 22 °C in PBS, followed by extensive dialysis to remove excess EGR-cmk. Matrix-assisted laser desorption ionization (MALDI) mass spectrometry of intact proteins in solution was conducted using reduced preparations (Alphalyse A/S, Odense, Denmark).

Amidolytic Assay of muPA Proteolytic Activity. The velocity of muPA-catalyzed hydrolysis of the chromogenic substrate L-pyroglutamyl-glycyl-L-arginine-*p*-nitroanilide hydrochloride (S-2444) (Aniara Diagnostica LLC, USA) was measured at 37 °C in HEPES-buffered saline (HBS; 10 mM HEPES, pH 7.4, 140 mM NaCl) with 0.1% bovine serum albumin (BSA) and enzyme and substrate concentrations as specified for each experiment. When antibody inhibition of the catalytic activity of muPA was measured, the enzyme (0.5 nM) was preincubated with various concentrations of mU1 (0−5 μM) in HBS at 22 °C for 15 min before adding S-2444, in concentrations as indicated for each single experiment. In all experiments, the initial reaction velocity was monitored at an absorbance of 405 nm (microplate reader).

Analysis of Plasmin-Mediated Cleavage of Single-Chain muPA. To analyze plasmin-catalyzed cleavage of single-chain muPA in the absence or presence of mU1, the single-chain muPA$^{(2-243)}$ (200 nM) variant, containing the residues GQKALRPRFK before the activation site at Ile16, was preincubated for 15 min at 22 °C with or without mU1 (1 μM) or control antibody mAb-112 (1 μM). At time 0, plasmin (5 nM final concentration) was added and the mixtures were incubated at 22 °C for 60, 30, 15, 10, 5, 2, or 0 min, respectively, after which the activity of plasmin was quenched by addition of aprotinin (1 μM final concentration). The amount of active two-chain muPA, generated by plasmin, was estimated by adding S-2444 (750 μM final concentration) and measuring the hydrolysis of S-2444 by monitoring the absorbance at 405 nm for 1 h at 37 °C. In addition, samples were taken from the incubation mixtures at each of the time points mentioned above and analyzed by nonreducing SDS−PAGE. The gel was stained with Coomassie Blue. The density of the stained bands were quantified by densitometry using the TotalLab Quant software, and the percentage of single-chain muPA$^{(2-243)}$, which had been converted to the two-chain muPA form, was plotted against the incubation time.

Surface Plasmon Resonance Measurements. To determine the equilibrium binding constants (K_D), the association rate constants (k_{on}), and dissociation rate constants (k_{off}) for antibody binding to muPA variants, surface plasmon resonance (SPR) analysis was conducted with a Biacore T200 instrument (GE Healthcare, Uppsala, Sweden). Polyclonal rabbit anti-mouse IgG from the Mouse Antibody Capture Kit (GE Healthcare, Uppsala, Sweden) was immobilized on a CM5 chip by amine coupling. Polyclonal rabbit anti-mouse IgG, at a concentration of 30 μg/mL in immobilization buffer (10 mM sodium acetate, pH 5.0), was injected over 7 min at a flow rate of 10 μL/min, until a level of ∼14 000 response units (RU) was reached, followed by surface blocking with ethanolamine. Antibody (mU1) in a running buffer (30 mM HEPES pH 7.4, 135 mM NaCl, and 0.1% bovine serum albumin) was then injected at a flow rate of 5 μL/min for 180 s until a capture level of ∼410 RU was reached. A flow cell without injection of mU1 was used as the reference. A dilution series of muPA variants (0−0.2 μM) in running buffer, purified on a benzamidine−Sepharose column immediately before the Biacore analysis, was injected over both flow cells at a flow rate of 30 μL/min during 240 s at 25 °C. Subsequently, the dissociation was monitored for 15 min. Kinetic constants (k_{on} and k_{off}) were calculated using the Biacore evaluation software to generate a 1:1 kinetic fit. The K_D values were calculated as k_{off}/k_{on}.

Measurement of Binding *p*-Aminobenzamidine to muPA by Fluorescence Spectroscopy. The binding of the fluorescent probe *p*-aminobenzamidine (*p*AB, Sigma) to the active site of full-length two-chain muPA was measured by modification of a previously described method.[25] Fluorescence emission spectra were recorded at 25 °C on a PTI Quantamaster spectrofluorophotometer in a 2 mm × 10 mm semimicro quartz cuvette in HBS (10 mM HEPES, pH 7.4, and 140 mM NaCl) with 0.1% polyethylene glycol 8000. Excitation was at 335 nm, and the emission was scanned from 340 to 400 nm. Equilibrium binding reactions were performed over a range of mU1 concentrations (0−1 μM) with 0.1 μM two-chain muPA in the presence of 20 μM *p*AB. Emission spectra were collected after 30 min of incubation with the use of an integration of 1−2 s over a 1.0 nm step resolution.

Quantitation of Incorporation of [^{3}H]-Diisopropyl-fluorophosphate (DFP) into muPA. [^{3}H]-DFP (50 μM) and C-terminally 6x histidine-tagged muPA$^{(16-243)}$ (100 nM) were incubated in the absence or presence of mU1 (0−1 μM) and C-terminally 6x histidine-tagged green fluorescent protein at a concentration of 1 mg/mL in HBS buffer. After 3 h at 22 °C, 100 μL of 50% Ni−Sepharose slurry was added to the 30 μL reaction mixture. The mixture was incubated for 30 min at 4 °C and washed four times in HBS buffer. The mixture was then transferred to scintillation liquid and bound (^{3}H-DFP) counted. Incubation of muPA$^{(16-243)}$ and [^{3}H]-DFP for 3 h in the absence of antibodies resulted in app 25% incorporation and was within the range of linearity between incorporation and time.

Carbamylation Assay. To analyze the effect of mU1 on the carbamylation rate of the N-terminal α-amino group of Ile16 in different muPA variants, the enzyme (0.5 μM) was preincubated with or without mU1 in HBS buffer, supplemented with 0.1% polyethylene glycol 8000, at 22 °C for 30 min. The full-length two-chain muPA variants were analyzed using a mU1 concentration of 1 μM. For muPA$^{(16-243)}$ analysis, a mU1 concentration of 0.5 μM was used. After preincubation, potassium cyanate (0.2 M) or HBS buffer supplemented with 0.1% polyethylene glycol 8000 was added and incubated at 22 °C for 0, 30, 60, 120, 180, and 300 min. To stop the

dx.doi.org/10.1021/bi400491k | *Biochemistry* 2013, 52, 7114−7126

carbamylation reaction, each of the mixtures was diluted 100 times in HBS supplemented with 0.1% BSA. mU1 was allowed to dissociate from muPA for 2 h at 22 °C. The residual activity was determined from the rate of hydrolysis of S-2444 (750 μM), by measuring absorbance at 405 nm at 37 °C for 1 h.

RESULTS

Mechanism of mU1 Inhibition of Activation of Single-Chain pro-muPA. It was previously shown that the monoclonal anti-muPA antibody mU1 inhibits plasmin-catalyzed activation of the inactive single-chain form of muPA.[22] We now wished to dissect the step in which the activation reaction is inhibited by the antibody. We therefore studied the effect of mU1 on plasmin-catalyzed cleavage of the Lys15−Ile16 peptide bond of purified single-chain muPA, using either full-length single-chain muPA (results not shown) or a variant of muPA (i.e., single-chain muPA$^{(2-243)}$) (Figure 2).

Initially, more than 95% of the purified protein appeared to be in the single-chain form, as judged by SDS−PAGE (Figure 2), and the specific activity (k_{cat}/K_M) was approximately 260 times lower than that of the two-chain activated form. In agreement with the previous results,[22] the activation of single-chain muPA$^{(2-243)}$ by plasmin, as measured using the peptidic S-2444 chromogenic substrate, was inhibited by mU1, whereas a control antibody, mAb-112, which is specific for human uPA,[24] had no effect (Figure 2A).

Unexpectedly, however, we observed no effect of the antibody on the cleavage of the single-chain form into the two-chain form by SDS−PAGE analysis (Figure 2B). Thus, mU1 inhibits activation (Figure 2A) but not cleavage of single-chain muPA (Figure 2B) (i.e., in the presence of mU1, cleavage of single-chain pro-muPA does not lead to the catalytically active form). To find out why mU1 inhibits plasmin-catalyzed activation of single-chain muPA, whereas plasmin-catalyzed cleavage of single-chain muPA was unaffected, we investigated whether mU1 could inhibit the catalytic activity of two-chain muPA with the chromogenic substrate S-2444. The measurements showed that mU1 inhibits the amidolytic activity of full-length two-chain muPA with an IC_{50} value around 50 nM (Figure 3A). The observed mU1-induced inhibition of active two-chain muPA fully explains why the single-chain proform, in a complex with mU1, does not become active after plasmin-catalyzed cleavage.

This finding may seem to conflict with Lund et al.[22] who reported that mU1 does not inhibit active two-chain muPA. However, the maximal mU1 concentration tested by Lund et al.[22] was 10 nM, at which concentration they observed a small, 10% inhibition. This results is fully in agreement with our result of a 50 nM IC_{50} (Figure 2). Also, Lund et al.[22] reported an IC_{50} of around 1 nM for mU1 inhibition of pro-muPA activation. This observation may also seem to conflict with the conclusion that pro-muPA activation is inhibited because mU1 inhibits the activity of the two-chain form, with an IC_{50} of 50 nM. However, once bound to pro-muPA with a high affinity, mU1 will dissociate very slowly, even from two-chain muPA (see below), implying that the equilibrium established during incubation of antibody and pro-muPA will determine the IC_{50} value even after conversion to the two-chain form. Again, the present data are fully in agreement with those of Lund et al.[22]

Kinetic Analysis of mU1 Inhibition of the Amidolytic Activity of Active Two-Chain muPA. To determine K_M^{app} and k_{cat}^{app} for S-2444 hydrolysis, initial velocities were measured in the presence or absence of mU1 and with 0−24 mM substrate

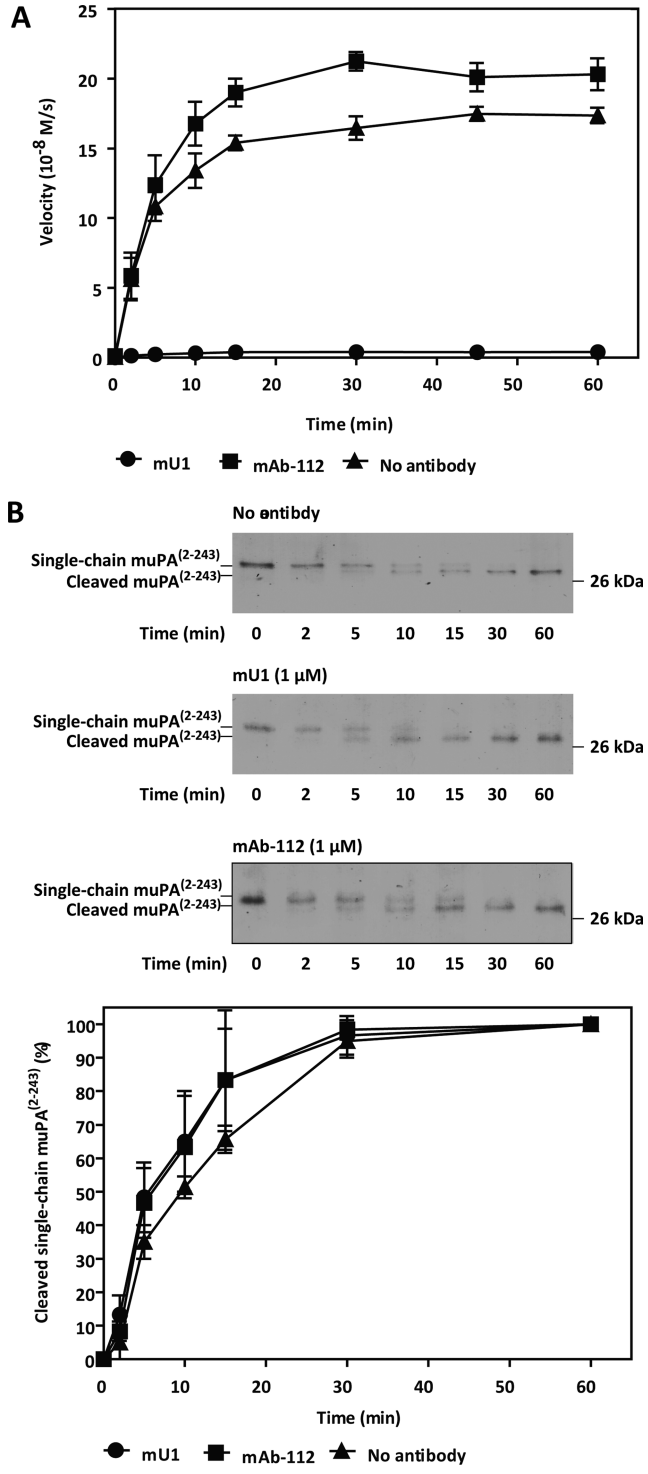

Figure 2. mU1 inhibits activation but not cleavage of single-chain muPA$^{(2-243)}$. (A) Rate of hydrolysis of S-2444 (750 μM) by 200 nM single-chain muPA$^{(2-243)}$ in the absence or presence of indicated antibodies (1 μM) after treatment with plasmin (5 nM) for the indicated time periods. (B) Nonreduced SDS−PAGE and Coomassie Blue staining of single-chain muPA$^{(2-243)}$ treated with plasmin under the same conditions as in (A). The migrations of single-chain and cleaved muPA$^{(2-243)}$ are indicated to the left. The migration of a M_r marker is indicated to the right. The densities of the stained bands were quantified by densitometry. The percentage of the single-chain muPA$^{(2-243)}$, which had been converted to the two-chain form, was plotted against the incubation time. All data are shown as means ± standard deviations of at least three independent determinations.

dx.doi.org/10.1021/bi400491k | Biochemistry 2013, 52, 7114−7126

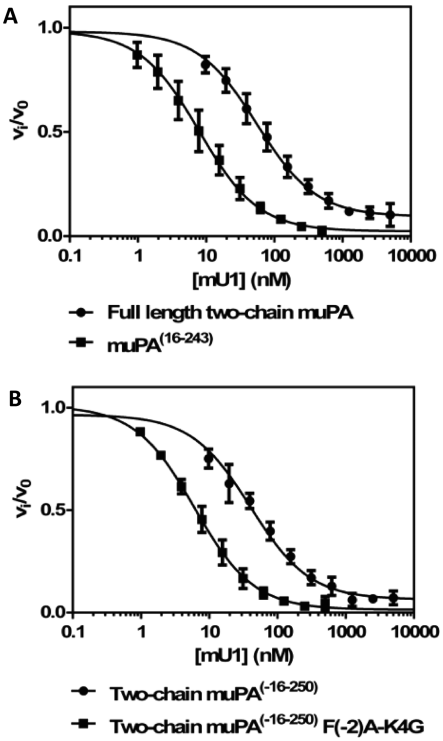

Figure 3. Inhibition of two-chain muPA by mU1. Rates of hydrolysis of S-2444 (750 μM) by 0.5 nM of (A) full-length two-chain muPA and muPA$^{(16-243)}$ and (B) two-chain muPA$^{(-16-250)}$ and two-chain muPA$^{(-16-250)}$ F(−2)A-K4G after preincubation with the indicated concentrations of mU1 (0−5 μM) are shown. The rates of hydrolysis were normalized to the rates in the absence of antibody for each muPA preparation. Means ± standard deviations of three determinations are indicated. Data were fitted to eq 2 to calculate K_D^{app}, v_0, and v_∞. The lines correspond to the fitted values. The fitted data for a number of independent determinations of K_D^{app} are listed in Table 2

($[S]_0$) and 0.5 nM muPA. The data were fitted to the following equation:

$$v = \frac{[E]_0 k_{cat.}^{app}[S]_0}{[S]_0 + K_M^{app}} \quad (1)$$

The calculated K_M^{app} values varied by 5−10% between different preparations of the same enzyme, whereas $k_{cat.}^{app}$, for unknown reasons, varied by 50−75% (results not shown). The measurements also showed that mU1 increased the K_M^{app} value for hydrolysis of S-2444 by full-length two-chain muPA, whereas $k_{cat.}^{app}$ was unaffected (Table 1). Therefore, these data suggest, as a first approximation, that mU1 is a competitive inhibitor of two-chain muPA. However, a more detailed analysis indicated a more complex mode of inhibition. First, plots of steady state velocities of the amidolytic activity against the concentration of mU1 demonstrated that full-length two-chain muPA was only inhibited by about 90% at saturating concentrations of mU1 (i.e., 5 μM) (Figure 3A). The residual activity was not due to contaminating proteases, as a specific peptidic inhibitor of muPA, mupain-1-16,[26] inhibited the activity completely (data not shown). The residual activity therefore seems to represent a true activity of the two-chain muPA−mU1 complex. Second, a truncated variant of muPA, muPA$^{(16-243)}$ (Figure 1) was previously demonstrated to assume a conformationally distorted state with a higher K_M^{app} for S-2444 hydrolysis than full-length two-chain muPA.[27] Surprisingly, we now found that the amidolytic activity of muPA$^{(16-243)}$ was inhibited with an IC_{50} value of only about 5 nM mU1, considerably lower than the IC_{50} value of about 50 nM determined for full-length two-chain muPA (Figure 3A). It was not possible to explain these findings by a competitive, uncompetitive, or a noncompetitive mode of inhibition of S-2444 hydrolysis by mU1.

For a quantitative treatment of these data, we considered a model in which two-chain muPA can equilibrate between two different states, an active one (E) and a distorted state (E*). The two forms are assumed to be in rapid equilibrium (equilibrium constants K_3 and K_4), and both forms are assumed to bind mU1 (here referred as I), but with different affinities (equilibrium dissociation constants K_1 and K_2):

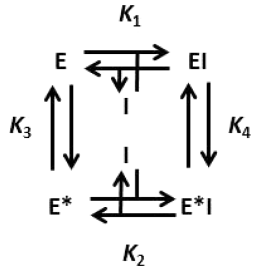

Establishing the equilibrium during a preincubation with the antibody, the enzyme activity is determined in an ensuing incubation with a chromogenic substrate. During the activity measurement, the antibody binding equilibrium is presumed to remain unchanged, due to the slow rates of antibody−muPA dissociation (Table 3). The reactions taking place are then defined by the following scheme:

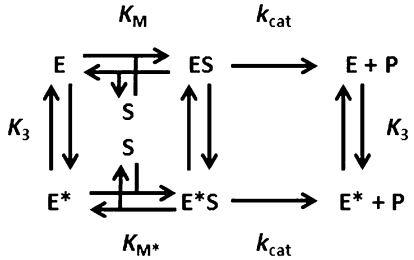

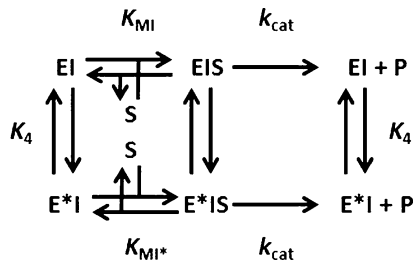

On the basis of the data in Table 1, $k_{cat.}^{app}$ does not vary with the mU1 concentration, whereas K_M^{app} does. The $k_{cat.}^{app}$ in these schemes is presumed to be identical for the different forms of the enzyme, whereas the K_M^{app} values are presumed to be variable. For these reaction schemes, one can derive (as described in the Supporting Information) the following equation for the dependence of the rate of substrate hydrolysis v on the antibody concentration [I]:

$$v = \frac{v_0 K_D^{app} + v_\infty[I]}{K_D^{app} + [I]} \quad (2)$$

dx.doi.org/10.1021/bi400491k | *Biochemistry* 2013, 52, 7114−7126

Table 1. K_M^{app} and $k_{cat.}^{app}$ for Full-Length Two-Chain muPA-Catalysed S-2444 Hydrolysis in the Presence of Varying Concentrations of mU1[a]

[mU1] (nM)	K_M^{app} (mM)	$k_{cat.}^{app}$ (s^{-1})
0	2.4 ± 0.2	124 ± 26
25	2.8 ± 0.1[b]	120 ± 30
50	3.6 ± 0.3[b]	125 ± 27
100	4.9 ± 1.1[b]	130 ± 25

[a]The K_M^{app} and $k_{cat.}^{app}$ values were determined by incubating full-length two-chain muPA (0.5 nM) with various concentrations of mU1 (0−100 nM) for 15 min at 22 °C before the addition of different concentrations of S-2444 (0−24 mM). Data were analysed according to Michaëlis−Menten kinetics. The table shows means ± standard deviations of at least three independent determinations. [b]Significantly different from the value for 0 nM mU1 ($p < 0.001$ by Student's t-test).

in which v_0 is the rate of substrate hydrolysis in the absence of inhibitor, v_∞ is the rate of substrate hydrolysis at indefinitely high inhibitor concentration, and K_D^{app} is the apparent equilibrium dissociation constant, which is related to the constants defined in the above scheme by the following equation:

$$K_D^{app} = K_2 \frac{(1 + K_3)}{(1 + K_4)} \quad (3)$$

The data obtained were fully in agreement with eq 2, including the fact that mU1 inhibited full-length two-chain muPA only down to 10% of the control value (Figure 3). The constants determined for full-length two-chain muPA, muPA$^{(16-243)}$, and two-chain muPA$^{(-16-250)}$ are listed in Table 2.

Table 2. K_M^{app} for S-2444 Hydrolysis and K_D^{app} for mU1 Inhibition for muPA Variants[a]

muPA variant	K_M^{app} (mM)	K_D^{app} (nM)
full-length two-chain muPA	2.4 ± 0.2	57 ± 14
muPA$^{(16-243)}$	5.0 ± 0.7[b]	8.3 ± 2.8[b]
full-length two-chain muPA F(−2)A-K4G	5.3 ± 0.2[b]	9.3 ± 0.6[b]
two-chain muPA$^{(-16-250)}$	2.3 ± 0.3	44 ± 12
two-chain muPA$^{(-16-250)}$ F(−2)A-K4G	4.1 ± 0.1[b]	7.5 ± 1.1[b]

[a]The K_M^{app} values were determined by measuring the rate of S-2444 hydrolysis by muPA variants (0.5 nM) at different concentrations of S-2444 (0−24 mM) and analysing the data according to Michaëlis−Menten kinetics. The K_D^{app} values were determined by measuring the rate of S-2444 (750 μM) hydrolysis in the presence of varying mU1 concentrations (0−5 μM) and analysing the data according to eq 2. The table shows means ± standard deviations for at least three independent determinations. [b]Significantly different from the value for full-length two-chain muPA ($p < 0.01$). All p-values were calculated by Student's t-test.

It is indicated that the K_D^{app} for binding to full-length two-chain muPA and two-chain muPA$^{(-16-250)}$ are around 50 nM, whereas that for muPA$^{(16-243)}$ is about 10 times lower.

The K_D^{app} values determined in this way, by inhibition of enzyme activity, are in good agreement with those determined by surface plasmon resonance (SPR) analysis (Table 3) on the basis of a 1:1 model. Importantly, reproducible fits to a 1:1 binding model in the case of two-chain muPA required purification of the enzyme on benzamidine−Sepharose immediately before the SPR. Interestingly, the variations in K_D values were almost totally accounted for by variations in k_{on}

Table 3. SPR Analysis of Binding of mU1 to Full-Length Two-Chain muPA and muPA Variants[a]

muPA variant	$k_{on} \times 10^{-5}$ (M^{-1} s^{-1})	$k_{off} \times 10^{4}$ (s^{-1})	K_D (nM)
full-length two-chain muPA	0.4 ± 0.0	7.4 ± 0.1	19 ± 1.2
muPA$^{(16-243)}$	1.1 ± 0.1[b]	7.1 ± 0.2	6.4 ± 0.9[b]
two-chain muPA$^{(-16-250)}$	0.2 ± 0.1	11.2 ± 2.8	60 ± 7.6[b]
single-chain muPA$^{(2-243)}$	6.6 ± 0.9[b]	5.8 ± 0.6	0.9 ± 0[b]

[a]Association rate (k_{on}), dissociation rate (k_{off}), and the equilibrium binding constants (K_D) of mU1 binding to full-length two-chain muPA and muPA variants were determined by fitting the SPR data to a 1:1 binding model. The data are reported as the means ± standard deviations of three independent determinations. [b]Significantly different from the value for full-length two-chain muPA ($p < 0.01$). All p-values were calculated by Student's t-test.

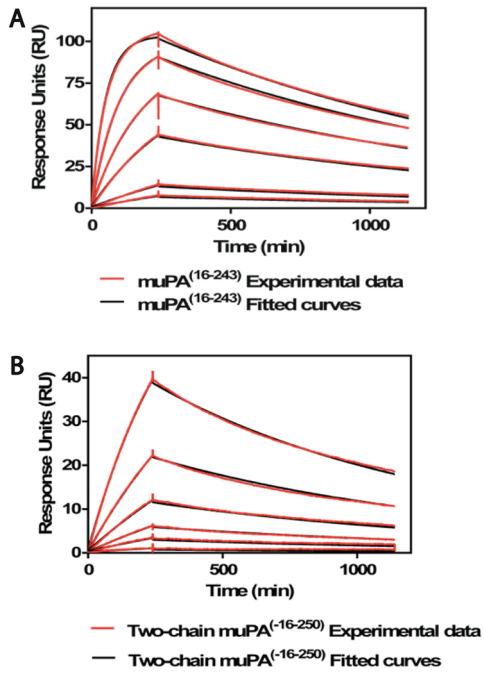

Figure 4. Surface plasmon resonance determination of the kinetics of binding of mU1 to muPA$^{(16-243)}$ and two-chain muPA$^{(-16-250)}$. Representative surface plasmon resonance sensorgrams for binding of mU1 to muPA$^{(16-243)}$ (A) and two-chain muPA$^{(-16-250)}$ (B). The experimental data (red curves) were fitted to a 1:1 binding model (black curves) with the Biacore evaluation software. The calculated k_{on}, k_{off}, and K_D values are listed in Table 3

(Figure 4 and Table 3). Also, the K_D value for the binding of mU1 to single-chain muPA$^{(2-243)}$ is 7 times lower than the K_D value for binding to muPA$^{(16-243)}$ and 20−60 times lower than binding to the longer muPA variants. Again, this variation is easily understood on the basis of the model proposed above and eq 3. A lower K_D^{app} value could result from a lower K_2 and/or a larger decrease of K_3 than of K_4. Alternatively, the presumed E* form and the zymogen may have different conformations, but both with a higher affinity to mU1 than the fully active (E) form.

The Epitope of mU1 is Located in the 37- and 70-Loops. Another anti-muPA monoclonal antibody, mU3, binds to an epitope in the 37- and 70-loops.[27] As it competes with mU1 for

dx.doi.org/10.1021/bi400491k | Biochemistry 2013, 52, 7114−7126

binding to full-length two-chain muPA,[22] the epitopes of mU1 and mU3 are likely to overlap. To determine the epitope of mU1, we analyzed the mU1 concentration dependency of inhibition of muPA-catalyzed S-2444 hydrolysis, using full-length two-chain muPA alanine substitution mutants in the 37- and 70-loops. As reported above, the K_D^{app} determined from the antibody concentration dependence of inhibition of full-length two-chain muPA by mU1 was about 50 nM (Table 2). However, the following 8 out of 30 mutants, namely G37cA, P37eA, P38A, K72A, S74A, Y76A, N77A, and P78A, all exhibited a reduced or completely abolished susceptibility to inhibition by 500 nM mU1 (Table 4), indicating that these

Table 4. Determination of the Epitope for mU1, As Measured by Determination of K_D^{app} Values for mU1 Inhibition of Point Mutants of Full-Length Two-Chain muPA[a]

muPA variant	K_D^{app} (nM)	K_M^{app} (mM)
full-length two-chain muPA	57 ± 14	2.4 ± 0.2
full-length two-chain muPA G37cA	>500[b]	2.5 ± 0.3
full-length two-chain muPA P37eA	>500[b]	2.1 ± 0.1
full-length two-chain muPA P38A	>500[b]	2.0 ± 0.2
full-length two-chain muPA K72A	>500[b]	2.5 ± 0.3
full-length two-chain muPA S74A	>500[b]	2.8 ± 0.0
full-length two-chain muPA Y76A	>500[b]	2.6 ± 0.2
full-length two-chain muPA N77A	>500[b]	3.7 ± 0.2[b]
full-length two-chain muPA P78A	>500[b]	2.2 ± 0.4

[a]Full-length two-chain muPA variants (0.5 nM) were preincubated with mU1 (0−500 nM) for 15 min at 22 °C, before measuring the S-2444 (750 μM) hydrolysis. Besides the values indicated in the table, the full-length two-chain muPA mutants E20A, F21A, T22A, E23A, Q35A, N37A, K37aA, G37bA, S37dA, K41A, H57A, Q60aA, E73A, S75A, Y93A, E96A, Y99A, T110A, S110aA, K143A, E146A, Y149A, L150A, K153A, N154A, and R217A were found to be inhibited by mU1 with K_D^{app} less than 2 times different from full-length two-chain muPA. Data are means ± standard deviations for at least three independent determinations. [b]Significantly different from the value for full-length two-chain muPA ($p < 0.005$ by Student's *t*-test).

eight residues are important for mU1 binding to full-length two-chain muPA. These eight mutants exhibited a K_M^{app} value for hydrolysis of S-2444 similar to full-length two-chain muPA (Table 1 and 4). The $k_{cat.}^{app}$ values for the different mutants were within 50−75%, but a similar variability was observed for different preparations of the same mutant (data not shown). We do not consider the $k_{cat.}^{app}$ values a relevant factor for comparing different enzyme preparations. We therefore concluded that the diminished binding to mU1 was not a result of misfolding. Key mutants (G37cA, P37eA, K72A, S74A, and P78A) were also tested by SPR and showed no measurable binding to mU1 (K_D > 500 nM). Altogether, these mutagenesis data mapped the epitope of mU1 to the 37- and 70-loops, located at least 20 Å from Lys72 C_α to Asp189 C_α in the S1 specificity pocket. Notably, mutation of a glycine (Gly37) and three prolines (Pro37e, Pro38, and Pro78) affected the binding, indicating that binding of mU1 depends on the conformation of the 37- and 70-loops. Overall, the residues implicated in the epitope cover a relatively large interaction surface of 923 Å^2 (Figure 5) compared to a typical antibody epitope, which is 680−880 Å^2.[28]

Phe(−2) and Lys4 in the A-chain Stabilize the Active Conformation of muPA. As described above, the truncated form of two-chain muPA, muPA$^{(16\text{-}243)}$, encoding only the B-chain (i.e., residues 16−250), has a much higher affinity for mU1 than full-length two-chain muPA and two-chain muPA$^{(\text{-}16\text{-}250)}$. In addition, the K_M^{app} value for S-2444 hydrolysis by muPA$^{(16\text{-}243)}$ is about 2 times higher than the K_M^{app} value for full-length two-chain muPA and two-chain muPA$^{(\text{-}16\text{-}250)}$ (Table 2). The residues responsible for these differences must be localized between residue −16 and 15. Alignment of residue −2 to 15 revealed strong interspecies conservation of particularly Phe(−2) and Lys4 (Figure 6A). Furthermore, in three-dimensional structures of human uPA, these two residues form contacts to the B-chain (Figure 6B,C). Substitution of Phe(−2) with Ala and of Lys4 with Gly led to an about 2 times increase in the K_M^{app} for S-2444 hydrolysis and a 5−10 times decrease in K_D^{app} for inhibition of S-2444 hydrolysis by mU1 (Table 2). The K_M^{app} for S-2444 hydrolysis was similar for the complex between mU1 and full-length two-chain muPA (Table 1) and full-length two-chain muPA F(−2)A-K4G double mutant in the absence of mU1 (Table 2). These data support the hypothesis of functional interactions between Phe(−2) and Lys4 in the A-chain and residues in the B-chain maintaining a maximally active state of the catalytic domain.

To verify that the part of the A-chain containing Phe(−2) and Lys4 was intact in the preparations used to draw these conclusions, we analyzed muPA$^{(-16-250)}$ (Figure 1), in which the A-chain was short enough to allow accurate mass determinations with MALDI mass spectrometry. Sequencing of two-chain muPA$^{(-16-250)}$ by Edman degradation revealed that the N-terminus was GSSLSKKP, as expected. Analysis of two-chain muPA$^{(-16-250)}$ and two-chain muPA$^{(-16-250)}$ F(−2A)/K4G by MALDI mass spectrometry under reducing conditions revealed an average mass of the B-chain for both proteins of 29.2 kDa, identical to the theoretical mass based on the sequence. For two-chain muPA$^{(-16-250)}$, the monoisotopic mass of the A-chain was found to be 25.91 kDa, corresponding to the sequence KPSSSVDQQGFQCGQ KALRPRFK. For two-chain muPA$^{(-16-250)}$ F(−2)A/K4G, the monoisotopic mass of the A-chain was found to be 30.04 kDa, corresponding to the sequence GSSLSKKPSSSVDQQGAQCGQ GALRPR-FK. It therefore appears that two-chain muPA$^{(-16-250)}$, but not two-chain muPA$^{(-16-250)}$ F(−2)A-K4G, was trimmed by removal of the N-terminal amino acids GSSLSK during the cleavage of the single-chain form by plasmin. Nevertheless, the MALDI analysis did show that the chain from residue −12 to 15 is indeed intact in both two-chain muPA$^{(-16-250)}$ and two-chain muPA$^{(-16-250)}$F(−2)A/K4G. The analysis also confirmed that the planned mutations were indeed introduced into the latter variant. We conclude that Phe(−2) and Lys4 stabilize the active conformation of two-chain muPA.

mU1 Induces Exposure of the N-terminus of the Catalytic Domain. Susceptibility to chemical carbamylation was previously used to measure exposure of the amino group of the N-terminal Ile16 of the catalytic domain of FVIIa and murine uPA.[27,29,30] The idea behind this analysis is that the amino group of Ile16 of a two-chain serine protease, such as full-length two-chain muPA, becomes susceptible to carbamylation, if it is even temporarily expelled from the activation pocket. The carbamylated Ile16 cannot reinsert, and the enzyme becomes permanently inactivated at a rate corresponding to the frequency of Ile16 exposure.

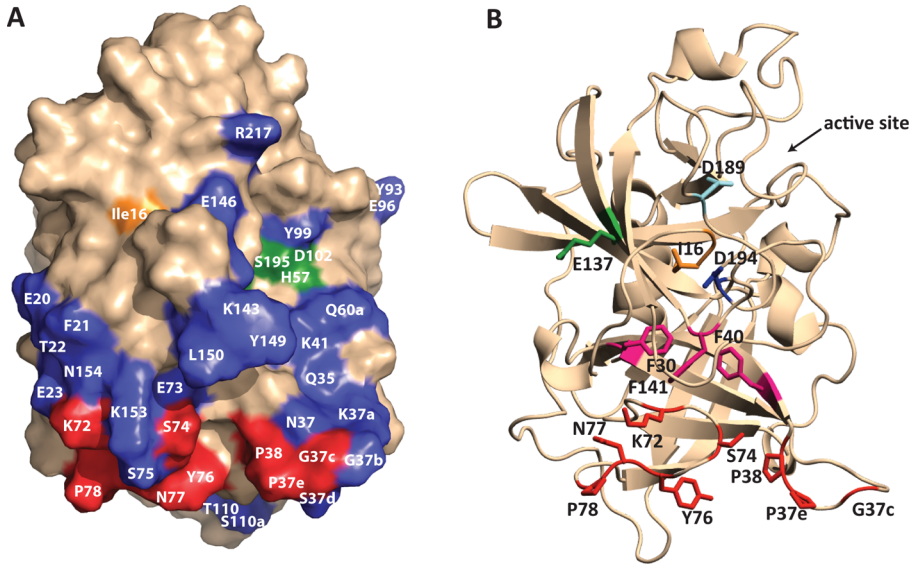

Figure 5. Epitope of mU1 on muPA. (A) Surface representation of the catalytic domain of muPA. Blue residues could be mutated to Ala without changing the K_D^{app} value for inhibition by mU1 by more than 2 times. Ala substitution of red residues increased the K_D^{app} value for inhibition and binding by mU1 by more than 2 times (see Table 4). The catalytic triad residues, His57, Asp102, and Ser195, are colored green, and the N-terminal Ile16, which is buried into the activation pocket, is marked by the adjacent Val17. The structure of the muPA catalytic domain was homology modeled by using Molecular Operating Environment software, the sequence of muPA (NP_032899.1), and the crystal structure of human uPA (PDB entry 2NWN) as the template.[12] (B) The model of murine uPA in ribbons with the epitope of mU1 is indicated in red sticks. Glu137 is shown in green. The Phe-cluster (Phe 30, 40, and 141) is magenta. Asp189 at the bottom of the S1 specificity pocket is cyan. Ile16, in orange, inserts into the activation pocket and forms a salt-bridge to Asp194, in blue.

As recently demonstrated,[27] full-length two-chain muPA is slowly inactivated by carbamylation, whereas muPA$^{(16-243)}$ is modified faster. The presence of mU1 enhanced the rate of Ile16 carbamylation of both full-length two-chain muPA and muPA$^{(16-243)}$ (Figure 7 and Table 5), indicating a shift in the equilibrium toward a state with the amino group of the Ile16 being exposed (Table 4). Hence, mU1 binding induces a distorted state with an exposed N-terminus Ile16. However, mU1 induces a more frequently exposed N-terminus in muPA$^{(16-243)}$ than in the full-length two-chain muPA, which indicates a more distorted state of the former.

The Active Site is Inaccessible Upon mU1 Binding. Fluorescence spectroscopy was used to measure the binding of *p*AB to full-length two-chain muPA[31] in the absence or presence of mU1 or the control antibody mAb-112. A mU1 concentration-dependent decrease in fluorescence, indicative of *p*AB displacement from the active site was observed (Figure 8A), whereas the control antibody (mAb-112) had no effect (data not shown). Hence, the mU1-induced conformational changes in muPA hinder binding of *p*AB to the active site of muPA.

Diisopropyl fluorophosphate (DFP) binds covalently to the hydroxyl group of Ser195 of active two-chain uPA.[27,32,33] Formation of the covalent bond requires an ordered oxyanion hole, as found only in the active state. Irreversible binding of [^{3}H]-DFP to the oxyanion hole of muPA$^{(16-243)}$ was inhibited in a dose-dependent manner by mU1, whereas the control antibody (mAb-112) did not affect the incorporation (Figure 8B).

These data indicate that both the S1 specificity pocket and the oxyanion hole of two-chain muPA are inaccessible in the complex with mU1.

DISCUSSION

Previous experiments demonstrated that mU1 can inhibit muPA in vivo.[22,23] We initiated this study to explain the mechanism by which mU1 inhibits activation of the single-chain zymogen form of muPA. We found that instead of abrogating the plasmin-catalyzed cleavage between Lys15 and Ile16 and the formation of the two-chain form, mU1 maintains the generated two-chain muPA in an inactive conformation. Nevertheless, our findings are in complete agreement with the original observation that the mU1 prevents plasmin-catalyzed activation of single-chain pro-muPA,[22] although the mechanism appears to be more complicated than originally assumed. Another potentially regulatory point (i.e., the binding of muPA to its cell surface receptor muPAR) has previously been shown not to be affected by mU1 neither in SPR analysis nor in cell binding assays.[22]

The fact that there is a distance of 20 Å between the epitope of mU1 and the active site of muPA suggests that mU1 inhibits the enzyme activity through a conformational transition. In the inactive state induced by mU1, the N-terminal Ile16 is solvent exposed, and the affinities for substrates and inhibitors are much lower than in the absence of mU1. Our present data are compatible with an equilibrium between an inactive and an active state, which is shifted toward the inactive state in the presence of mU1 and also, although less so, in the absence of residues −16 to 15.

Derivatisation of the various muPA variants with EGR-cmk or the presence of a high concentration of *p*AB reduced the affinity to mU1 maximally 2 times (data not shown). This observation is in good agreement with previous observations with human uPA. Thus, human single-chain pro-uPA could be labeled with 5-(dimethylamino)-1-naphthalenesulfonyl (dansyl)-EGR-cmk in the presence of dipeptides mimicking the activating residues 16 and 17 of the catalytic domain, but upon removal of the dipeptide, the dansyl-EGR-cmk-derivatized molecule again assumed a zymogen conformation.[24,34] In this respect, uPA seems to differ from FVIIa, with which peptide-cmk

dx.doi.org/10.1021/bi400491k | *Biochemistry* 2013, 52, 7114−7126

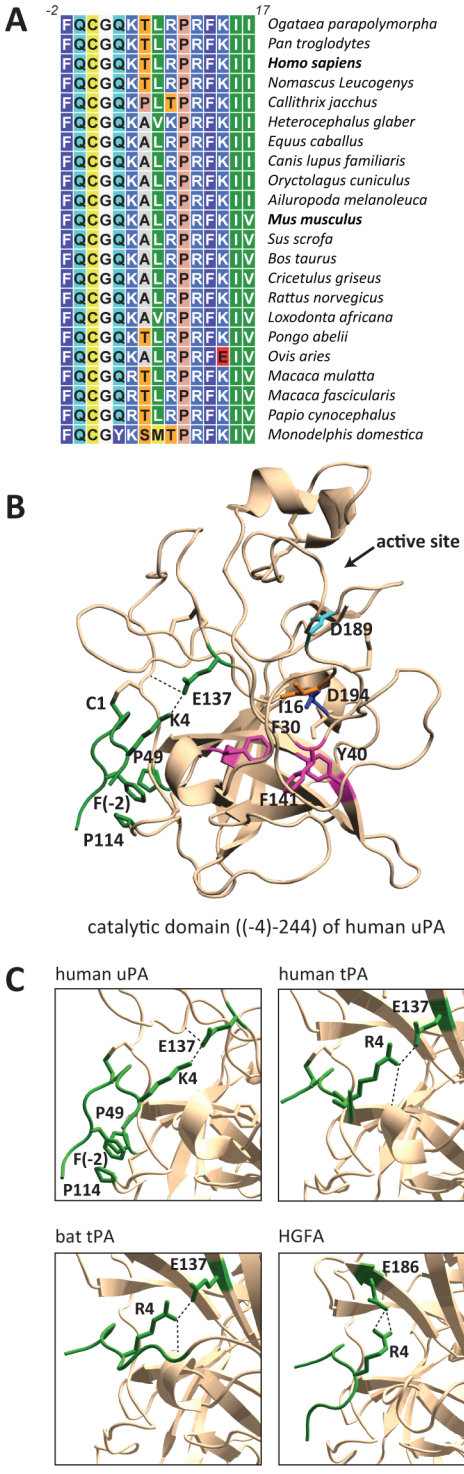

Figure 6. Phe(−2) and Lys4 in A-chain interact with residues in B-chain. (A) Multiple sequence alignment of residues −2 to 17 of uPA from different species. Residues are colored according to their physical−chemical properties and murine and human sequences are indicated in bold. (B) X-ray crystal structure of human uPA from PDB entry 1C5W. (C) The hydrogen bond from the side-chain of residue 4 in crystal structures of human uPA (1C5W),[64] human tPA (1RTF),[60] bat tPA (1A5I),[61] and HGFA (1YBW).[49] (B) and (C) Residues important for the allosteric regulation of uPA are shown in green. Residues corresponding to the Phe-cluster in murine uPA are magenta. Asp189, at the bottom of the S1 specificity pocket, is cyan. Ile16, in orange, indicates the activation pocket in which it forms a salt-bridge to Asp194, in blue.

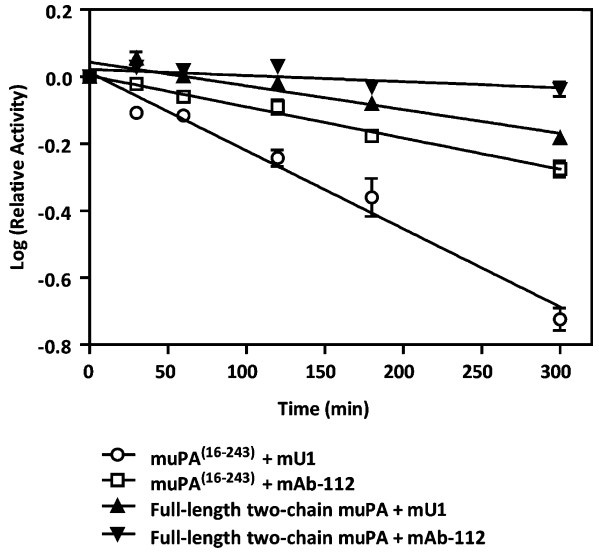

Figure 7. Carbamylation rate measurements reveal enhanced exposure of amino group of N-terminal Ile16 of muPA upon binding of mU1. The figure shows the rates of activity loss following carbamylation of full-length two-chain muPA and muPA$^{(16-243)}$ in absence or presence of mU1, as indicated. The relative activity at each time point is calculated as the fractional activity compared to time point 0. Data are the means ± standard deviations of at least three independent determinations. The rate constants for the activity loss are shown in Table 5

Table 5. Effects of mU1 on Rates of Carbamylation of muPA Variants[a]

muPA variant	rate × 10^{-4} (min^{-1})
full-length two-chain muPA	2.4 ± 0.9
full-length two-chain muPA + mU1	7.1 ± 0.2[b]
full-length two-chain muPA + mAb-112	2.9 ± 0.2
muPA$^{(16-243)}$	9.3 ± 1.0[b]
muPA$^{(16-243)}$ + mU1	22.8 ± 1.6[b]
muPA$^{(16-243)}$ + mAb-112	9.7 ± 1.4[b]

[a]Data are the means ± standard deviations of at least three independent determinations. [b]Significantly different from the value for full-length two-chain muPA ($p < 0.001$ by Student's t-test).

derivatives can affect the K_D for binding to conformation-specific antibodies more than 100 times.[35,36]

On the basis of these observations and our previous study,[27] we suggest that the herein demonstrated mU1-induced distorted state resembles the distorted E* conformation observed in three-dimensional structures of other serine proteases. In the absence of ligands, an equilibrium between active and distorted inactive E* forms has been identified in several serine proteases.[37] In thrombin, the E* state is characterized by a collapse of the 215−217 segment, with Trp215 closing the S1 entrance frame.[38−41] Collapsed structures with a blocked active site have been observed not only in thrombin but also in complement factor I[42] and D,[43,44] prostate specific kallikrein,[45] prostasin,[46] αI-tryptase,[47] DegP,[48] and HGFA.[49] Similarly, collapsed forms are also observed in zymogens of pro-granzyme K,[50] chymotrypsinogen,[51] plasminogen,[52] complement profactor D,[53] prokallikrein 6,[54] complement pro-factor C1r,[55] and prethrombin-1.[56]

Binding of mU1 to full-length two-chain muPA leads to an increase in the K_M^{app}, whereas $k_{cat.}^{app}$ remains unchanged (Table 1). A previously described monoclonal antibody, mAb-112, binds

dx.doi.org/10.1021/bi400491k | Biochemistry 2013, 52, 7114−7126

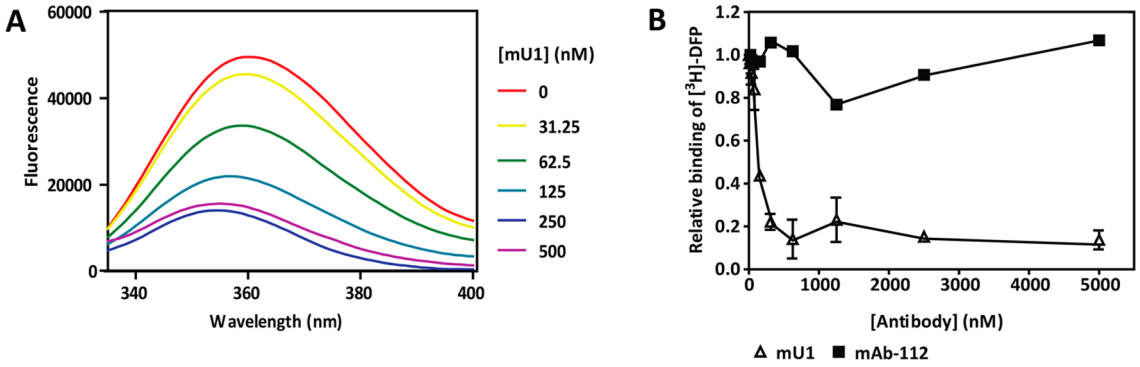

Figure 8. The S1 specificity pocket and oxyanion hole are inaccessible in the presence of mU1. (A) Binding of *p*AB (20 μM) to full-length two-chain muPA (100 nM) in the presence of different concentrations of mU1 (0−500 nM), as determined by fluorescence spectroscopy. The result is a representative of at least three independent determinations (B) Incorporation of [^{3}H]-DFP (50 μM) into muPA$^{(16-243)}$ (100 nM) for a 3 h incubation with the indicated concentrations of antibodies. Data are represented as the fractional binding compared to the sample without mU1. Data are means ± standard deviations of at least three independent determinations.

to human uPA and induces a zymogen-like conformation.[21,24] In contrast to mU1, mAb-112 is an apparently noncompetitive inhibitor, reducing $k_{cat.}^{app}$ without affecting K_M^{app}. As based on the enzyme kinetics, the mU1-induced state of two-chain muPA therefore, seems to be different from the mAb-112-induced state of human uPA. In addition, the epitope for mU1 is located in the 37- and 70-loops, whereas that of mAb-112 is localized in the autolysis loop (residues 142−152). But similarly to mAb-112, the variations in affinity of mU1 to specific conformations (full-length two-chain muPA, muPA$^{(16-243)}$, and single-chain muPA$^{(2-243)}$) are associated with variations in k_{on}, but not k_{off}, as measured by SPR (Table 3 and Figure 4). This observation is in good agreement with expectancies from a model, in which the antibodies bind to a pre-existing but variably populated conformation in the various enzyme preparations. In addition, X-ray crystal structure analysis of the complex between two-chain human uPA and a Fab fragment of mAb-112 showed that the S1 pocket of the enzyme is occluded, owing to a 9.7 Å displacement of the peptide segment Trp215−Arg217 and burial of the Arg217 side chain in the pocket,[21] similar to the E* states referred to above. Understanding the exact relation of the mU1-full-length muPA complex and muPA$^{(16-243)}$ to the E* conformations and the zymogen conformation will, however, have to await X-ray crystal structure analysis of an mU1-muPA complex. In general, the exact relationship between the E* conformation and zymogen conformation is a matter of debate.[57,58]

The fact that mU1 has a higher affinity for the target in the absence of the −16 to 15 residue stretch may give clues to its mechanism of action. According to our data, Phe(−2) and Lys4 stabilize the structure of the catalytic domain in the active conformation. Residues in the region from position −2 to 15 of uPA are highly conserved among mammalian species, particularly Phe(−2) and Lys4 (Figure 6A). Several three-dimensional structures of the catalytic domain of human uPA have been solved from crystals of proteins containing this stretch of residues (Figure 6B). Phe(−2) engages in a hydrophobic interaction with Pro49 and Pro114 in human uPA, and both residues are conserved in muPA. Lys4 points inward, away from the solvent, forming a hydrogen bond to Glu137. Moreover, in active human single-chain and two-chain tissue-type plasminogen activator (tPA), bat tPA as well as HGFA (Figure 6C), Arg4 forms a similar hydrogen bond.[49,59−61] Accordingly, the quenching of these interactions by our mutations of muPA gives rise to a conformational change of the catalytic domain, which increases the affinity to mU1. One may therefore hypothesize that the residues contacting Phe(−2) and Lys4 may be involved in the communication between the mU1 epitope and the active site. There is an extended hydrogen bonding network encompassing the activation loop, the 70-loop, the autolysis loop, and Asp194. A hydrophobic cluster composed of Phe30, Phe40, and Phe141 may also contribute to the coupling between the A-chain, the active site, and the autolysis loop. Disruption of the Lys4−Gly137 interaction could therefore affect the integrity of the activation pocket.

The inhibitory mechanism suggested here is completely different from the mechanism that can be derived from the crystal structure of the allosteric antibody hH35 in complex with hepsin[20] and the crystal structure of the allosteric antibody FAb40 in complex with HGFA.[19] The antibody hH35 binds to the 170-loop of hepsin and inhibits noncompetitively, whereas Fab40 binds to HGFA in the vicinity of the 99-loop and acts through a partially competitive inhibition mechanism. The functional epitope of mU1 is located more than 20 Å away from the active site of muPA compared to the distance of 15−20 Å reported for the structural epitope of hH35 on hepsin.[20] Hence, its mode of inhibition and the long distance from the epitope to the active site makes the inhibitory mechanism of mU1 distinct from those of hH35 and Fab40.

Epitope mapping revealed overlapping binding sites for mU1 (Figure 5) and mU3,[27] which is intriguing in light of the different functional effects of these two antibodies. The difference can be explained by the assumption that the enzyme exists in active and inactive distorted states in equilibrium with each other. The epitopes of the two antibodies may have different conformations in the different states, and the two antibodies lock the active and distorted, inactive states, respectively. Binding to one of the antibodies, mU1, shifts the equilibrium in the direction of the inactive, distorted state, whereas binding of the other antibody, mU3, shifts the equilibrium toward the active state. This assumption is in agreement with the observation that the two antibodies have slightly different epitopes. Lys72 and Pro78 were only a part of the mU1 epitope and not of the mU3 epitope. Furthermore, residues in the 37-loop are relatively more important for binding of mU3 than residues in the 70-loop. Compared to the inhibition mechanism of mU1, the slightly different epitope of

dx.doi.org/10.1021/bi400491k | *Biochemistry* 2013, 52, 7114−7126

mU3 seemingly causes an opposite effect, in which the enzyme is stabilized in the active conformation instead of the distorted one, implying stabilization of the N-terminal Ile16 in the activation pocket and ordering of the active site. A similar situation has been reported with two antibodies (mAb-112 and mAb-12E6B10) binding to an overlapping epitope in human uPA.[62] Although both mAb-112 and mAb-12E6B10 inhibited uPA-catalyzed plasminogen activation, only mAb-112 induced a zymogen-like conformation in the enzyme.

Certain naturally occurring mutations in the region of thrombin with homology to position −2 to 15 of uPA cause serious bleeding phenotypes in patients, whereas mutation of Arg4 affects the proteolytic activity of thrombin.[63] According to our data, proteolytic degradation of the region encompassing Phe(−2) and Lys4 or yet to be identified naturally occurring mutations of these residues in muPA and most likely other serine proteases, would favor a distorted state. Although such regulatory mechanisms remain to be identified, they may exist in vivo, under normal or pathological conditions. The presence of this distorted conformation in vivo is not only interesting from a mechanistic point of view but also because it improves the possibilities of therapeutic targeting of uPA. Conversion to the E* state is a new mode of pharmacological intervention with serine protease activity. mU1 is the first antibody described to stabilize this distorted state in a serine protease by targeting the 37- and 70-loops.

■ ASSOCIATED CONTENT

Supporting Information

Derivatisation of formulas describing mU1 inhibition of murine urokinase-type plasminogen activator (uPA) are described in Figure S1. This material is available free of charge via the Internet at http://pubs.acs.org.

■ AUTHOR INFORMATION

Corresponding Author

*T. Kromann-Hansen. Gustav Wieds Vej 10C, DK-8000 Aarhus C, Denmark, Tel.: (+45) 87154907. E-mail: tobiaskh@mb.au.dk.

Funding

This work was supported by grants from the Danish Cancer Society (DP 07043, DP 08001); the Danish National Research Foundation (26-331-6); the Danish Research Agency (272-06-0518); the Novo Nordisk Foundation (R114-A11382); and the Lundbeck Foundation (R83-A7826).

Notes

The authors declare no competing financial interest.

■ ABBREVIATIONS

DFP, diisopropyl fluorophosphate; EGR-cmk, glutamyl-glycyl-arginyl-chloromethyl ketone; HBS, HEPES-buffered saline; HGFA, hepatocyte growth factor activator; MALDI, matrix assisted laser desorption/ionization; muPA, murine urokinase-type plasminogen activator; *p*AB, *p*-aminobenzamidine; PBS, phosphate-buffered saline; PEI, polyethyleneimine; RU, response unit; SPR, surface plasmon resonance; tPA, tissue-type plasminogen activator; uPA, urokinase-type plasminogen activator; uPAR, urokinase-type plasminogen activator receptor

■ ADDITIONAL NOTE

[a]Template numbering which is based on chymotrypsin[11]. Residues N-terminal to Cys1 are negatively numbered, for example Phe(−2).

■ REFERENCES

(1) Andreasen, P. A., Egelund, R., and Petersen, H. H. (2000) The plasminogen activation system in tumor growth, invasion, and metastasis. *Cell. Mol. Life Sci. 57*, 25−40.

(2) Danø, K., Behrendt, N., Høyer-Hansen, G., Johnsen, M., Lund, L. R., Ploug, M., and Rømer, J. (2005) Plasminogen activation and cancer. *Thromb. Haemostasis 93*, 676−681.

(3) Hildenbrand, R., Allgayer, H., Marx, A., and Stroebel, P. (2010) Modulators of the urokinase-type plasminogen activation system for cancer. *Expert Opin. Invest. Drugs 19*, 641−652.

(4) Lund, I. K., Illemann, M., Thurison, T., Christensen, I. J., and Høyer-Hansen, G. (2011) uPAR as anti-cancer target: evaluation of biomarker potential, histological localization, and antibody-based therapy. *Curr. Drug Targets 12*, 1744−1760.

(5) Ellis, V., Scully, M. F., and Kakkar, V. V. (1989) Plasminogen activation initiated by single-chain urokinase-type plasminogen activator. Potentiation by U937 monocytes. *J. Biol. Chem. 264*, 2185−2188.

(6) Petersen, L. C., Lund, L. R., Nielsen, L. S., Danø, K., and Skriver, L. (1988) One-chain urokinase-type plasminogen activator from human sarcoma cells is a proenzyme with little or no intrinsic activity. *J. Biol. Chem. 263*, 11189−11195.

(7) Bode, W., Schwager, P., and Huber, R. (1978) The transition of bovine trypsinogen to a trypsin-like state upon strong ligand binding. The refined crystal structures of the bovine trypsinogen-pancreatic trypsin inhibitor complex and of its ternary complex with Ile-Val at 1.9 A resolution. *J. Mol. Biol. 118*, 99−112.

(8) Hedstrom, L. (2002) Serine protease mechanism and specificity. *Chem. Rev. 102*, 4501−4524.

(9) Page, M. J., and Di Cera, E. (2008) Serine peptidases: classification, structure and function. *Cell. Mol. Life Sci. 65*, 1220−1236.

(10) Perona, J. J., and Craik, C. S. (1995) Structural basis of substrate specificity in the serine proteases. *Protein Sci. 4*, 337−360.

(11) Spraggon, G., Phillips, C., Nowak, U. K., Ponting, C. P., Saunders, D., Dobson, C. M., Stuart, D. I., and Jones, E. Y. (1995) The crystal structure of the catalytic domain of human urokinase-type plasminogen activator. *Structure 3*, 681−691.

(12) Zhao, G., Yuan, C., Wind, T., Huang, Z., Andreasen, P. A., and Huang, M. (2007) Structural basis of specificity of a peptidyl urokinase inhibitor, upain-1. *J. Struct. Biol. 160*, 1−10.

(13) Schweinitz, A., Steinmetzer, T., Banke, I. J., Arlt, M. J., Sturzebecher, A., Schuster, O., Geissler, A., Giersiefen, H., Zeslawska, E., Jacob, U., Krüger, A., and Sturzebecher, J. (2004) Design of novel and selective inhibitors of urokinase-type plasminogen activator with improved pharmacokinetic properties for use as antimetastatic agents. *J. Biol. Chem. 279*, 33613−33622.

(14) Coussens, L. M., Fingleton, B., and Matrisian, L. M. (2002) Matrix metalloproteinase inhibitors and cancer: trials and tribulations. *Science 295*, 2387−2392.

(15) Adams, G. P., and Weiner, L. M. (2005) Monoclonal antibody therapy of cancer. *Nat. Biotechnol. 23*, 1147−1157.

(16) Nelson, A. L., Dhimolea, E., and Reichert, J. M. (2010) Development trends for human monoclonal antibody therapeutics. *Nat. Rev. Drug Discovery 9*, 767−774.

(17) Petersen, H. H., Hansen, M., Schousboe, S. L., and Andreasen, P. A. (2001) Localization of epitopes for monoclonal antibodies to urokinase-type plasminogen activator: relationship between epitope localization and effects of antibodies on molecular interactions of the enzyme. *Eur. J. Biochem. 268*, 4430−4439.

(18) Ganesan, R., Eigenbrot, C., and Kirchhofer, D. (2010) Structural and mechanistic insight into how antibodies inhibit serine proteases. *Biochem. J. 430*, 179−189.

(19) Ganesan, R., Eigenbrot, C., Wu, Y., Liang, W. C., Shia, S., Lipari, M. T., and Kirchhofer, D. (2009) Unraveling the allosteric mechanism of serine protease inhibition by an antibody. *Structure 17*, 1614−1624.
(20) Koschubs, T., Dengl, S., Durr, H., Kaluza, K., Georges, G., Hartl, C., Jennewein, S., Lanzendorfer, M., Auer, J., Stern, A., Huang, K. S., Packman, K., Gubler, U., Kostrewa, D., Ries, S., Hansen, S., Kohnert, U., Cramer, P., and Mundigl, O. (2012) Allosteric antibody inhibition of human hepsin protease. *Biochem. J. 442*, 483−494.
(21) Jiang, L., Botkjaer, K. A., Andersen, L. M., Yuan, C., Andreasen, P. A., and Huang, M. (2013) Rezymogenation of active urokinase induced by an inhibitory antibody. *Biochem. J. 449*, 161−166.
(22) Lund, I. K., Jögi, A., Rønø, B., Rasch, M. G., Lund, L. R., Almholt, K., Gårdsvoll, H., Behrendt, N., Rømer, J., and Høyer-Hansen, G. (2008) Antibody-mediated targeting of the urokinase-type plasminogen activator proteolytic function neutralizes fibrinolysis in vivo. *J. Biol. Chem. 283*, 32506−32515.
(23) Jögi, A., Rønø, B., Lund, I. K., Nielsen, B. S., Ploug, M., Høyer-Hansen, G., Rømer, J., and Lund, L. R. (2010) Neutralisation of uPA with a monoclonal antibody reduces plasmin formation and delays skin wound healing in tPA-deficient mice. *PloS one 5*, e12746.
(24) Blouse, G. E., Bøtkjaer, K. A., Deryugina, E., Byszuk, A. A., Jensen, J. M., Mortensen, K. K., Quigley, J. P., and Andreasen, P. A. (2009) A novel mode of intervention with serine protease activity: targeting zymogen activation. *J. Biol. Chem. 284*, 4647−4657.
(25) Olson, S. T., Bock, P. E., Kvassman, J., Shore, J. D., Lawrence, D. A., Ginsburg, D., and Bjork, I. (1995) Role of the catalytic serine in the interactions of serine proteinases with protein inhibitors of the serpin family. Contribution of a covalent interaction to the binding energy of serpin-proteinase complexes. *J. Biol. Chem. 270*, 30007−30017.
(26) Hosseini, M., Jiang, L., Sørensen, H. P., Jensen, J. K., Christensen, A., Fogh, S., Yuan, C., Andersen, L. M., Huang, M., Andreasen, P. A., and Jensen, K. J. (2011) Elucidation of the contribution of active site and exosite interactions to affinity and specificity of peptidylic serine protease inhibitors using non-natural arginine analogs. *Mol. Pharmacol. 80*, 585−597.
(27) Liu, Z., Kromann-Hansen, T., Lund, I. K., Hosseini, M., Jensen, K. J., Høyer-Hansen, G., Andreasen, P. A., and Sørensen, H. P. (2012) Interconversion of active and inactive conformations of urokinase-type plasminogen activator. *Biochemistry 51*, 7804−7811.
(28) Jin, L., Fendly, B. M., and Wells, J. A. (1992) High resolution functional analysis of antibody-antigen interactions. *J. Mol. Biol. 226*, 851−865.
(29) Higashi, S., Matsumoto, N., and Iwanaga, S. (1996) Molecular mechanism of tissue factor-mediated acceleration of factor VIIa activity. *J. Biol. Chem. 271*, 26569−26574.
(30) Higashi, S., Nishimura, H., Aita, K., and Iwanaga, S. (1994) Identification of regions of bovine factor VII essential for binding to tissue factor. *J. Biol. Chem. 269*, 18891−18898.
(31) Jiang, L., Svane, A. S., Sørensen, H. P., Jensen, J. K., Hosseini, M., Chen, Z., Weydert, C., Nielsen, J. T., Christensen, A., Yuan, C., Jensen, K. J., Nielsen, N. C., Malmendal, A., Huang, M., and Andreasen, P. A. (2011) The Binding Mechanism of a Peptidic Cyclic Serine Protease Inhibitor. *J. Mol. Biol. 412*, 235−250.
(32) Nielsen, L. S., Hansen, J. G., Skriver, L., Wilson, E. L., Kaltoft, K., Zeuthen, J., and Danø, K. (1982) Purification of zymogen to plasminogen activator from human glioblastoma cells by affinity chromatography with monoclonal antibody. *Biochemistry 21*, 6410−6415.
(33) Jansen, E. F., Nutting, F., and Balls, A. K. (1949) Mode of inhibition of chymotrypsin by diisopropyl fluorophosphate; introduction of phosphorus. *J. Biol. Chem. 179*, 201−204.
(34) Bøtkjaer, K. A., Byszuk, A. A., Andersen, L. M., Christensen, A., Andreasen, P. A., and Blouse, G. E. (2009) Nonproteolytic induction of catalytic activity into the single-chain form of urokinase-type plasminogen activator by dipeptides. *Biochemistry 48*, 9606−9617.
(35) Dickinson, C. D., Shobe, J., and Ruf, W. (1998) Influence of cofactor binding and active site occupancy on the conformation of the macromolecular substrate exosite of factor VIIa. *J. Mol. Biol. 277*, 959−971.
(36) Andersen, L. M., Andreasen, P. A., Svendsen, I., Keemink, J., Østergaard, H., and Persson, E. (2012) Antibody-induced enhancement of factor VIIa activity through distinct allosteric pathways. *J. Biol. Chem. 287*, 8994−9001.
(37) Gohara, D. W., and Di Cera, E. (2011) Allostery in trypsin-like proteases suggests new therapeutic strategies. *Trends Biotechnol. 29*, 577−585.
(38) Niu, W., Chen, Z., Bush-Pelc, L. A., Bah, A., Gandhi, P. S., and Di Cera, E. (2009) Mutant N143P reveals how Na+ activates thrombin. *J. Biol. Chem. 284*, 36175−36185.
(39) Gandhi, P. S., Chen, Z., Mathews, F. S., and Di Cera, E. (2008) Structural identification of the pathway of long-range communication in an allosteric enzyme. *Proc. Natl. Acad. Sci. U. S. A. 105*, 1832−1837.
(40) Pineda, A. O., Chen, Z. W., Bah, A., Garvey, L. C., Mathews, F. S., and Di Cera, E. (2006) Crystal structure of thrombin in a self-inhibited conformation. *J. Biol. Chem. 281*, 32922−32928.
(41) Bah, A., Carrell, C. J., Chen, Z., Gandhi, P. S., and Di Cera, E. (2009) Stabilization of the E* form turns thrombin into an anticoagulant. *J. Biol. Chem. 284*, 20034−20040.
(42) Roversi, P., Johnson, S., Caesar, J. J., McLean, F., Leath, K. J., Tsiftsoglou, S. A., Morgan, B. P., Harris, C. L., Sim, R. B., and Lea, S. M. (2011) Structural basis for complement factor I control and its disease-associated sequence polymorphisms. *Proc. Natl. Acad. Sci. U. S. A. 108*, 12839−12844.
(43) Jing, H., Babu, Y. S., Moore, D., Kilpatrick, J. M., Liu, X. Y., Volanakis, J. E., and Narayana, S. V. (1998) Structures of native and complexed complement factor D: implications of the atypical His57 conformation and self-inhibitory loop in the regulation of specific serine protease activity. *J. Mol. Biol. 282*, 1061−1081.
(44) Narayana, S. V., Carson, M., el-Kabbani, O., Kilpatrick, J. M., Moore, D., Chen, X., Bugg, C. E., Volanakis, J. E., and DeLucas, L. J. (1994) Structure of human factor D. A complement system protein at 2.0 A resolution. *J. Mol. Biol. 235*, 695−708.
(45) Carvalho, A. L., Sanz, L., Barettino, D., Romero, A., Calvete, J. J., and Romao, M. J. (2002) Crystal structure of a prostate kallikrein isolated from stallion seminal plasma: a homologue of human PSA. *J. Mol. Biol. 322*, 325−337.
(46) Rickert, K. W., Kelley, P., Byrne, N. J., Diehl, R. E., Hall, D. L., Montalvo, A. M., Reid, J. C., Shipman, J. M., Thomas, B. W., Munshi, S. K., Darke, P. L., and Su, H. P. (2008) Structure of human prostasin, a target for the regulation of hypertension. *J. Biol. Chem. 283*, 34864−34872.
(47) Rohr, K. B., Selwood, T., Marquardt, U., Huber, R., Schechter, N. M., Bode, W., and Than, M. E. (2006) X-ray structures of free and leupeptin-complexed human alphaI-tryptase mutants: indication for an alpha−>beta-tryptase transition. *J. Mol. Biol. 357*, 195−209.
(48) Krojer, T., Garrido-Franco, M., Huber, R., Ehrmann, M., and Clausen, T. (2002) Crystal structure of DegP (HtrA) reveals a new protease-chaperone machine. *Nature 416*, 455−459.
(49) Shia, S., Stamos, J., Kirchhofer, D., Fan, B., Wu, J., Corpuz, R. T., Santell, L., Lazarus, R. A., and Eigenbrot, C. (2005) Conformational lability in serine protease active sites: structures of hepatocyte growth factor activator (HGFA) alone and with the inhibitory domain from HGFA inhibitor-1B. *J. Mol. Biol. 346*, 1335−1349.
(50) Hink-Schauer, C., Estebanez-Perpina, E., Wilharm, E., Fuentes-Prior, P., Klinkert, W., Bode, W., and Jenne, D. E. (2002) The 2.2-A crystal structure of human pro-granzyme K reveals a rigid zymogen with unusual features. *J. Biol. Chem. 277*, 50923−50933.
(51) Freer, S. T., Kraut, J., Robertus, J. D., Wright, H. T., and Xuong, N. H. (1970) Chymotrypsinogen: 2.5-angstrom crystal structure, comparison with alpha-chymotrypsin, and implications for zymogen activation. *Biochemistry 9*, 1997−2009.
(52) Peisach, E., Wang, J., de los Santos, T., Reich, E., and Ringe, D. (1999) Crystal structure of the proenzyme domain of plasminogen. *Biochemistry 38*, 11180−11188.
(53) Jing, H., Macon, K. J., Moore, D., DeLucas, L. J., Volanakis, J. E., and Narayana, S. V. (1999) Structural basis of profactor D activation: from a highly flexible zymogen to a novel self-inhibited serine protease, complement factor D. *EMBO J. 18*, 804−814.

(54) Gomis-Rüth, F. X., Bayes, A., Sotiropoulou, G., Pampalakis, G., Tsetsenis, T., Villegas, V., Aviles, F. X., and Coll, M. (2002) The structure of human prokallikrein 6 reveals a novel activation mechanism for the kallikrein family. *J. Biol. Chem. 277*, 27273−27281.
(55) Budayova-Spano, M., Grabarse, W., Thielens, N. M., Hillen, H., Lacroix, M., Schmidt, M., Fontecilla-Camps, J. C., Arlaud, G. J., and Gaboriaud, C. (2002) Monomeric structures of the zymogen and active catalytic domain of complement protease c1r: further insights into the c1 activation mechanism. *Structure 10*, 1509−1519.
(56) Chen, Z., Pelc, L. A., and Di Cera, E. (2010) Crystal structure of prethrombin-1. *Proc. Natl. Acad. Sci. U. S. A. 107*, 19278−19283.
(57) Huntington, J. A. (2009) Slow thrombin is zymogen-like . *J. Thromb. Haemostasis 7* (Suppl 1), 159−164.
(58) Pozzi, N., Vogt, A. D., Gohara, D. W., and Di Cera, E. (2012) Conformational selection in trypsin-like proteases. *Curr. Opin. Struct. Biol. 22*, 421−431.
(59) Renatus, M., Engh, R. A., Stubbs, M. T., Huber, R., Fischer, S., Kohnert, U., and Bode, W. (1997) Lysine 156 promotes the anomalous proenzyme activity of tPA: X-ray crystal structure of single-chain human tPA. *EMBO J. 16*, 4797−4805.
(60) Lamba, D., Bauer, M., Huber, R., Fischer, S., Rudolph, R., Kohnert, U., and Bode, W. (1996) The 2.3 A crystal structure of the catalytic domain of recombinant two-chain human tissue-type plasminogen activator. *J. Mol. Biol. 258*, 117−135.
(61) Renatus, M., Stubbs, M. T., Huber, R., Bringmann, P., Donner, P., Schleuning, W. D., and Bode, W. (1997) Catalytic domain structure of vampire bat plasminogen activator: a molecular paradigm for proteolysis without activation cleavage. *Biochemistry 36*, 13483−13493.
(62) Botkjaer, K. A., Fogh, S., Bekes, E. C., Chen, Z., Blouse, G. E., Jensen, J. M., Mortensen, K. K., Huang, M., Deryugina, E., Quigley, J. P., Declerck, P. J., and Andreasen, P. A. (2011) Targeting the autolysis loop of urokinase-type plasminogen activator with conformation-specific monoclonal antibodies. *Biochem. J. 438*, 39−51.
(63) Papaconstantinou, M. E., Bah, A., and Di Cera, E. (2008) Role of the A chain in thrombin function. *Cell. Mol. Life Sci. 65*, 1943−1947.
(64) Katz, B. A., Mackman, R., Luong, C., Radika, K., Martelli, A., Sprengeler, P. A., Wang, J., Chan, H., and Wong, L. (2000) Structural basis for selectivity of a small molecule, S1-binding, submicromolar inhibitor of urokinase-type plasminogen activator. *Chem. Biol. 7*, 299−312.